

PAPER • OPEN ACCESS

Measurement of Ξ_{cc}^{++} production in pp collisions at $\sqrt{s} = 13$ TeV

You may also like

- [Future Physics Programme of BESIII](#)
M. Ablikim, M. N. Achasov, P. Adlarson et al.

To cite this article: LHCb Collaboration *et al* 2020 *Chinese Phys. C* **44** 022001

View the [article online](#) for updates and enhancements.

Measurement of Ξ_{cc}^{++} production in pp collisions at $\sqrt{s} = 13$ TeV*

LHCb Collaboration

R. Aaij³¹ C. Abellán Beteta⁴⁹ T. Ackernley⁵⁹ B. Adeva⁴⁵ M. Adinolfi⁵³ H. Afsharnia⁹ C.A. Aidala⁸⁰
 S. Aiola²⁵ Z. Ajaltouni⁹ S. Akar⁶⁶ P. Albicocco²² J. Albrecht¹⁴ F. Alessio⁴⁷ M. Alexander⁵⁸
 A. Alfonso Alberio⁴⁴ G. Alkhazov³⁷ P. Alvarez Cartelle⁶⁰ A.A. Alves Jr⁴⁵ S. Amato² Y. Amhis¹¹ L. An²¹
 L. Anderlini²¹ G. Andreassi⁴⁸ M. Andreotti²⁰ F. Archilli¹⁶ A. Artamonov⁴³ M. Artuso⁶⁷ K. Arzymatov⁴¹
 E. Aslanides¹⁰ M. Atzeni⁴⁹ B. Audurier²⁶ S. Bachmann¹⁶ J.J. Back⁵⁵ S. Baker⁶⁰ V. Balagura^{11,b}
 W. Baldini^{20,47} A. Baranov⁴¹ R.J. Barlow⁶¹ S. Barsuk¹¹ W. Barter⁶⁰ M. Bartolini^{23,47,h} F. Baryshnikov⁷⁷
 J.M. Basels¹³ G. Bassi²⁸ V. Batozskaya³⁵ B. Batsukh⁶⁷ A. Battig¹⁴ A. Bay⁴⁸ M. Becker¹⁴ F. Bedeschi²⁸
 I. Bediaga¹ A. Beiter⁶⁷ L.J. Bel³¹ V. Belavin⁴¹ S. Belin²⁶ V. Bellec⁴⁸ K. Belous⁴³ I. Belyaev³⁸
 G. Bencivenni²² E. Ben-Haim¹² S. Benson³¹ S. Beranek¹³ A. Berezhnoy³⁹ R. Bernet⁴⁹ D. Berninghoff¹⁶
 H.C. Bernstein⁶⁷ C. Bertella⁴⁷ E. Bertholet¹² A. Bertolin²⁷ C. Betancourt⁴⁹ F. Betti^{19,e} M.O. Bettler⁵⁴
 Ia. Bezshyiko⁴⁹ S. Bhasin⁵³ J. Bhom³³ M.S. Bieker¹⁴ S. Bifani⁵² P. Billoir¹² A. Bizzeti^{21,u} M. Bjørn⁶²
 M.P. Blago⁴⁷ T. Blake⁵⁵ F. Blanc⁴⁸ S. Blusk⁶⁷ D. Bobulska⁵⁸ V. Bocci³⁰ O. Boente Garcia⁴⁵ T. Boettcher⁶³
 A. Boldyrev⁷⁸ A. Bondar^{42,x} N. Bondar³⁷ S. Borghi^{61,47} M. Borisyak⁴¹ M. Borsato¹⁶ J.T. Borsuk³³
 T.J.V. Bowcock⁵⁹ C. Bozzi²⁰ M.J. Bradley⁶⁰ S. Braun¹⁶ A. Brea Rodriguez⁴⁵ M. Brodski⁴⁷ J. Brodzicka³³
 A. Brossa Gonzalo⁵⁵ D. Brundu²⁶ E. Buchanan⁵³ A. Buonauro⁴⁹ C. Burr⁴⁷ A. Bursche²⁶ A. Butkevich⁴⁰
 J.S. Butter³¹ J. Buytaert⁴⁷ W. Byczynski⁴⁷ S. Cadeddu²⁶ H. Cai⁷² R. Calabrese^{20,g} L. Calero Diaz²² S. Cali²²
 R. Calladine⁵² M. Calvi^{24,i} M. Calvo Gomez^{44,m} P. Camargo Magalhaes⁵³ A. Camboni^{44,m} P. Campana²²
 D.H. Campora Perez³¹ A.F. Campoverde Quezada⁵ L. Capriotti^{19,e} A. Carbone^{19,e} G. Carboni²⁹ R. Cardinale^{23,h}
 A. Cardini²⁶ I. Carli⁶ P. Carniti^{24,i} K. Carvalho Akiba³¹ A. Casais Vidal⁴⁵ G. Casse⁵⁹ M. Cattaneo⁴⁷
 G. Cavallero⁴⁷ S. Celani⁴⁸ R. Cenci^{28,p} J. Cerasoli¹⁰ M.G. Chapman⁵³ M. Charles^{12,47} Ph. Charpentier⁴⁷
 G. Chatzikonstantinidis⁵² M. Chefdeville⁸ V. Chekalina⁴¹ C. Chen³ S. Chen²⁶ A. Chernov³³ S.-G. Chitic⁴⁷
 V. Chobanova⁴⁵ S. Cholak⁴⁸ M. Chruszcz³³ A. Chubykin³⁷ P. Ciambone²² M.F. Cicala⁵⁵ X. Cid Vidal⁴⁵
 G. Ciezarek⁴⁷ F. Cindolo¹⁹ P.E.L. Clarke⁵⁷ M. Clemencic⁴⁷ H.V. Cliff⁵⁴ J. Closier⁴⁷ J.L. Cobbedick⁶¹
 V. Coco⁴⁷ J.A.B. Coelho¹¹ J. Cogan¹⁰ E. Cogneras⁹ L. Cojocariu³⁶ P. Collins⁴⁷ T. Colombo⁴⁷
 A. Comerma-Montells¹⁶ A. Contu²⁶ N. Cooke⁵² G. Coombs⁵⁸ S. Coquereau⁴⁴ G. Corti⁴⁷ C.M. Costa Sobral⁵⁵
 B. Couturier⁴⁷ D.C. Craik⁶³ J. Crkovska⁶⁶ A. Crocombe⁵⁵ M. Cruz Torres^{1,ab} R. Currie⁵⁷ C.L. Da Silva⁶⁶
 E. Dall'Occo¹⁴ J. Dalseno^{45,53} C. D'Ambrosio⁴⁷ A. Danilina³⁸ P. d'Argent⁴⁷ A. Davis⁶¹
 O. De Aguiar Francisco⁴⁷ K. De Bruyn⁴⁷ S. De Capua⁶¹ M. De Cian⁴⁸ J.M. De Miranda¹ L. De Paula²
 M. De Serio^{18,d} P. De Simone²² J.A. de Vries³¹ C.T. Dean⁶⁶ W. Dean⁸⁰ D. Decamp⁸ L. Del Buono¹²
 B. Delaney⁵⁴ H.-P. Dembinski¹⁵ A. Dendek³⁴ V. Denysenko⁴⁹ D. Derkach⁷⁸ O. Deschamps⁹ F. Desse¹¹
 F. Dettori²⁶ B. Dey⁷ A. Di Canto⁴⁷ P. Di Nezza²² S. Didenko⁷⁷ H. Dijkstra⁴⁷ V. Dobishuk⁵¹ F. Dordei²⁶

Received 25 October 2019, Published online 31 December 2019

* Supported by CERN and national agencies: CAPES, CNPq, FAPERJ and FINEP (Brazil); MOST and NSFC (China); CNRS/IN2P3 (France); BMBF, DFG and MPG (Germany); INFN (Italy); NWO (Netherlands); MNiSW and NCN (Poland); MEN/IFA (Romania); MSHE (Russia); MinECo (Spain); SNSF and SER (Switzerland); NASU (Ukraine); STFC (United Kingdom); DOE NP and NSF (USA). We acknowledge the computing resources that are provided by CERN, IN2P3 (France), KIT and DESY (Germany), INFN (Italy), SURF (Netherlands), PIC (Spain), GridPP (United Kingdom), RRCKI and Yandex LLC (Russia), CSCS (Switzerland), IFIN-HH (Romania), CBPF (Brazil), PL-GRID (Poland) and OSC (USA). We are indebted to the communities behind the multiple open-source software packages on which we depend. Individual groups or members have received support from AvH Foundation (Germany); EPLANET, Marie Skłodowska-Curie Actions and ERC (European Union); ANR, Labex P2IO and OCEVU, and Région Auvergne-Rhône-Alpes (France); Key Research Program of Frontier Sciences of CAS, CAS PIFI, and the Thousand Talents Program (China); RFBR, RSF and Yandex LLC (Russia); GVA, XuntaGal and GENCAT (Spain); the Royal Society and the Leverhulme Trust (United Kingdom).



Content from this work may be used under the terms of the Creative Commons Attribution 3.0 licence. Any further distribution of this work must maintain attribution to the author(s) and the title of the work, journal citation and DOI. Article funded by SCOAP³ and published under licence by Chinese Physical Society and the Institute of High Energy Physics of the Chinese Academy of Sciences and the Institute of Modern Physics of the Chinese Academy of Sciences and IOP Publishing Ltd

M. Dorigo^{28,y} A.C. dos Reis¹ L. Douglas⁵⁸ A. Dovbnya⁵⁰ K. Dreimanis⁵⁹ M.W. Dudek³³ L. Dufour⁴⁷
 G. Dujany¹² P. Durante⁴⁷ J.M. Durham⁶⁶ D. Dutta⁶¹ M. Dziewiecki¹⁶ A. Dziurda³³ A. Dzyuba³⁷ S. Easo⁵⁶
 U. Egede⁶⁹ V. Egorychev³⁸ S. Eidelman^{42,x} S. Eisenhardt⁵⁷ R. Ekelhof¹⁴ S. Ek-In⁴⁸ L. Eklund⁵⁸ S. Ely⁶⁷
 A. Ene³⁶ E. Epple⁶⁶ S. Escher¹³ S. Esen³¹ T. Evans⁴⁷ A. Falabella¹⁹ J. Fan³ N. Farley⁵² S. Farry⁵⁹
 D. Fazzini¹¹ P. Fedin³⁸ M. Féo⁴⁷ P. Fernandez Declara⁴⁷ A. Fernandez Prieto⁴⁵ F. Ferrari^{19,e} L. Ferreira Lopes⁴⁸
 F. Ferreira Rodrigues² S. Ferreres Sole³¹ M. Ferrillo⁴⁹ M. Ferro-Luzzi⁴⁷ S. Filippov⁴⁰ R.A. Fini¹⁸
 M. Fiorini^{20,g} M. Firllej³⁴ K.M. Fischer⁶² C. Fitzpatrick⁴⁷ T. Fiutowski³⁴ F. Fleuret^{11,b} M. Fontana⁴⁷
 F. Fontanelli^{23,h} R. Forty⁴⁷ V. Franco Lima⁵⁹ M. Franco Sevilla⁶⁵ M. Frank⁴⁷ C. Frei⁴⁷ D.A. Friday⁵⁸ J. Fu^{25,q}
 M. Fuehring¹⁴ W. Funk⁴⁷ E. Gabriel⁵⁷ A. Gallas Torreira⁴⁵ D. Galli^{19,e} S. Gallorini²⁷ S. Gambetta⁵⁷
 Y. Gan³ M. Gandelman² P. Gandini²⁵ Y. Gao⁴ L.M. Garcia Martin⁴⁶ J. García Pardiñas⁴⁹ B. Garcia Plana⁴⁵
 F.A. Garcia Rosales¹¹ L. Garrido⁴⁴ D. Gascon⁴⁴ C. Gaspar⁴⁷ D. Gerick¹⁶ E. Gersabeck⁶¹ M. Gersabeck⁶¹
 T. Gershon⁵⁵ D. Gerstel¹⁰ Ph. Ghez⁸ V. Gibson⁵⁴ A. Gioventù⁴⁵ O.G. Girard⁴⁸ P. Gironella Gironell⁴⁴
 L. Giubega³⁶ C. Giugliano²⁰ K. Gizdov⁵⁷ V.V. Gligorov¹² C. Göbel⁷⁰ D. Golubkov³⁸ A. Golutvin^{60,77}
 A. Gomes^{1,a} P. Gorbounov^{38,6} I.V. Gorelov³⁹ C. Gotti^{24,i} E. Govorkova³¹ J.P. Grabowski¹⁶ R. Graciani Diaz⁴⁴
 T. Grammatico¹² L.A. Granado Cardoso⁴⁷ E. Graugés⁴⁴ E. Graverini⁴⁸ G. Graziani²¹ A. Grecu³⁶ R. Greim³¹
 P. Griffith²⁰ L. Grillo⁶¹ L. Gruber⁴⁷ B.R. Gruberg Cazon⁶² C. Gu³ E. Gushchin⁴⁰ A. Guth¹³ Yu. Guz^{43,47}
 T. Gys⁴⁷ P. A. Günther¹⁶ T. Hadavizadeh⁶² G. Haefeli⁴⁸ C. Haen⁴⁷ S.C. Haines⁵⁴ P.M. Hamilton⁶⁵ Q. Han⁷
 X. Han¹⁶ T.H. Hancock⁶² S. Hansmann-Menzemer¹⁶ N. Harnew⁶² T. Harrison⁵⁹ R. Hart³¹ C. Hasse¹⁴
 M. Hatch⁴⁷ J. He⁵ M. Hecker⁶⁰ K. Heijhoff³¹ K. Heinicke¹⁴ A.M. Hennequin⁴⁷ K. Hennessy⁵⁹ L. Henry⁴⁶
 J. Heuel¹³ A. Hicheur⁶⁸ D. Hill⁶² M. Hilton⁶¹ P.H. Hopchev⁴⁸ J. Hu¹⁶ W. Hu⁷ W. Huang⁵ W. Hulsbergen³¹
 T. Humair⁶⁰ R.J. Hunter⁵⁵ M. Hushchyn⁷⁸ D. Hutchcroft⁵⁹ D. Hynds³¹ P. Ibis¹⁴ M. Idzik³⁴ P. Ilten⁵²
 A. Inglessi³⁷ K. Ivshin³⁷ R. Jacobsson⁴⁷ S. Jakobsen⁴⁷ E. Jans³¹ B.K. Jashal⁴⁶ A. Jawahery⁶⁵ V. Jevtic¹⁴
 F. Jiang³ M. John⁶² D. Johnson⁴⁷ C.R. Jones⁵⁴ B. Jost⁴⁷ N. Jurik⁶² S. Kandybei⁵⁰ M. Karacson⁴⁷
 J.M. Kariuki⁵³ N. Kazeev⁷⁸ M. Kecke¹⁶ F. Keizer^{54,47} M. Kelsey⁶⁷ M. Kenzie⁵⁵ T. Ketel³² B. Khanji⁴⁷
 A. Kharisova⁷⁹ K.E. Kim⁶⁷ T. Kim¹³ V.S. Kirsebom⁴⁸ S. Klaver²² K. Klimaszewski³⁵ S. Koliiev⁵¹
 A. Kondybayeva⁷⁷ A. Konoplyannikov³⁸ P. Kopciwicz³⁴ R. Kopečna¹⁶ P. Koppenburg³¹ I. Kostjuk^{31,51}
 O. Kot⁵¹ S. Kotriakhova³⁷ L. Kravchuk⁴⁰ R.D. Krawczyk⁴⁷ M. Kreps⁵⁵ F. Kress⁶⁰ S. Kretschmar¹³
 P. Krokovny^{42,x} W. Krupa³⁴ W. Krzemien³⁵ W. Kucewicz^{33,1} M. Kucharczyk³³ V. Kudryavtsev^{42,x}
 H.S. Kuindersma³¹ G.J. Kunde⁶⁶ T. Kvaratskheliya³⁸ D. Lacarrere⁴⁷ G. Lafferty⁶¹ A. Lai²⁶ D. Lancierini⁴⁹
 J.J. Lane⁶¹ G. Lanfranchi²² C. Langenbruch¹³ O. Lantwin⁴⁹ T. Latham⁵⁵ F. Lazzari^{28,v} C. Lazzeroni⁵²
 R. Le Gac¹⁰ R. Lefèvre⁹ A. Leflat³⁹ O. Leroy¹⁰ T. Lesiak³³ B. Leverington¹⁶ H. Li⁷¹ L. Li⁶² X. Li⁶⁶
 Y. Li⁶ Z. Li⁶⁷ X. Liang⁶⁷ R. Lindner⁴⁷ V. Lisovskyi¹⁴ G. Liu⁷¹ X. Liu³ D. Loh⁵⁵ A. Loi²⁶
 J. Lomba Castro⁴⁵ I. Longstaff⁵⁸ J.H. Lopes² G. Loustau⁴⁹ G.H. Lovell⁵⁴ Y. Lu⁶ D. Lucchesi^{27,o}
 M. Lucio Martinez³¹ Y. Luo³ A. Lupato²⁷ E. Luppi^{20,g} O. Lupton⁵⁵ A. Lusiani^{28,t} X. Lyu⁵ S. Maccolini^{19,e}
 F. Machefer¹¹ F. Maciuc³⁶ V. Macko⁴⁸ P. Mackowiak¹⁴ S. Maddrell-Mander⁵³ L.R. Madhan Mohan⁵³
 O. Maev^{37,47} A. Maevskiy⁷⁸ D. Maisuzenko³⁷ M.W. Majewski³⁴ S. Malde⁶² B. Malecki⁴⁷ A. Malinin⁷⁶
 T. Maltsev^{42,x} H. Malygina¹⁶ G. Manca^{26,f} G. Mancinelli¹⁰ R. Manera Escalero⁴⁴ D. Manuzzi^{19,e}
 D. Marangotto^{25,q} J. Maratas^{9,w} J.F. Marchand⁸ U. Marconi¹⁹ S. Mariani²¹ C. Marin Benito¹¹ M. Marinangeli⁴⁸
 P. Marino⁴⁸ J. Marks¹⁶ P.J. Marshall⁵⁹ G. Martellotti³⁰ L. Martinazzoli⁴⁷ M. Martinelli^{24,i}
 D. Martinez Santos⁴⁵ F. Martinez Vidal⁴⁶ A. Massafferri¹ M. Materok¹³ R. Matev⁴⁷ A. Mathad⁴⁹ Z. Mathe⁴⁷
 V. Matiunin³⁸ C. Matteuzzi²⁴ K.R. Mattioli⁸⁰ A. Mauri⁴⁹ E. Maurice^{11,b} M. McCann⁶⁰ L. McConnell¹⁷
 A. McNab⁶¹ R. McNulty¹⁷ J.V. Mead⁵⁹ B. Meadows⁶⁴ C. Meaux¹⁰ G. Meier¹⁴ N. Meinert⁷⁴ D. Melnychuk³⁵
 S. Meloni^{24,i} M. Merk³¹ A. Merli²⁵ M. Mikhasenko⁴⁷ D.A. Milanes⁷³ E. Millard⁵⁵ M.-N. Minard⁸
 O. Mineev³⁸ L. Minzoni^{20,g} S.E. Mitchell⁵⁷ B. Mitreska⁶¹ D.S. Mitzel⁴⁷ A. Mödden¹⁴ A. Mogini¹²
 R.D. Moise⁶⁰ T. Mombächer¹⁴ I.A. Monroy⁷³ S. Monteil⁹ M. Morandin²⁷ G. Morello²² M.J. Morello^{28,t}
 J. Moron³⁴ A.B. Morris¹⁰ A.G. Morris⁵⁵ R. Mountain⁶⁷ H. Mu³ F. Muheim⁵⁷ M. Mukherjee⁷ M. Mulder⁴⁷

D. Müller⁴⁷ K. Müller⁴⁹ C.H. Murphy⁶² D. Murray⁶¹ P. Muzzetto²⁶ P. Naik⁵³ T. Nakada⁴⁸ R. Nandakumar⁵⁶
 T. Nanut⁴⁸ I. Nasteva² M. Needham⁵⁷ N. Neri^{25,q} S. Neubert¹⁶ N. Neufeld⁴⁷ R. Newcombe⁶⁰ T.D. Nguyen⁴⁸
 C. Nguyen-Mau^{48,n} E.M. Niel¹¹ S. Nieswand¹³ N. Nikitin³⁹ N.S. Nolte⁴⁷ C. Nunez⁸⁰ A. Oblakowska-
 Mucha³⁴ V. Obraztsov⁴³ S. Ogilvy⁵⁸ D.P. O'Hanlon⁵³ R. Oldeman^{26,f} C.J.G. Onderwater⁷⁵ J. D. Osborn⁸⁰
 A. Ossowska³³ J.M. Otalora Goicochea² T. Ovsiannikova³⁸ P. Owen⁴⁹ A. Oyanguren⁴⁶ P.R. Pais⁴⁸ T. Pajero^{28,t}
 A. Palano¹⁸ M. Palutan²² G. Panshin⁷⁹ A. Papanestis⁵⁶ M. Pappagallo⁵⁷ L.L. Pappalardo^{20,g}
 C. Pappenheimer⁶⁴ W. Parker⁶⁵ C. Parkes⁶¹ G. Passaleva^{21,47} A. Pastore¹⁸ M. Patel⁶⁰ C. Patrignani^{19,e}
 A. Pearce⁴⁷ A. Pellegrino³¹ M. Pepe Altarelli⁴⁷ S. Perazzini¹⁹ D. Pereima³⁸ P. Perret⁹ L. Pescatore⁴⁸
 K. Petridis⁵³ A. Petrolini^{23,h} A. Petrov⁷⁶ S. Petrucci⁵⁷ M. Petruzzo^{25,q} B. Pietrzyk⁸ G. Pietrzyk⁴⁸ M. Pili⁶²
 D. Pinci³⁰ J. Pinzino⁴⁷ F. Pisani¹⁹ A. Piucci¹⁶ V. Placinta³⁶ S. Playfer⁵⁷ J. Plews⁵² M. Plo Casaus⁴⁵
 F. Polci¹² M. Poli Lener²² M. Poliakov⁶⁷ A. Poluektov¹⁰ N. Polukhina^{77,c} I. Polyakov⁶⁷ E. Polycarpo²
 G.J. Pomery⁵³ S. Ponce⁴⁷ A. Popov⁴³ D. Popov⁵² S. Poslavskii⁴³ K. Prasanth³³ L. Promberger⁴⁷ C. Prouve⁴⁵
 V. Pugatch⁵¹ A. Puig Navarro⁴⁹ H. Pullen⁶² G. Punzi^{28,p} W. Qian⁵ J. Qin⁵ R. Quagliani¹² B. Quintana⁸
 N.V. Raab¹⁷ R.I. Rabadan Trejo¹⁰ B. Rachwal³⁴ J.H. Rademacker⁵³ M. Rama²⁸ M. Ramos Pernas⁴⁵
 M.S. Rangel² F. Ratnikov^{41,78} G. Raven³² M. Reboud⁸ F. Redi⁴⁸ F. Reiss¹² C. Remon Alepuz⁴⁶ Z. Ren³
 V. Renaudin⁶² S. Ricciardi⁵⁶ D.S. Richards⁵⁶ S. Richards⁵³ K. Rinnert⁵⁹ P. Robbe¹¹ A. Robert¹²
 A.B. Rodrigues⁴⁸ E. Rodrigues⁶⁴ J.A. Rodriguez Lopez⁷³ M. Roehrken⁴⁷ S. Roiser⁴⁷ A. Rollings⁶²
 V. Romanovskiy⁴³ M. Romero Lamas⁴⁵ A. Romero Vidal⁴⁵ J.D. Roth⁸⁰ M. Rotondo²² M.S. Rudolph⁶⁷ T. Ruf⁴⁷
 J. Ruiz Vidal⁴⁶ A. Ryzhikov⁷⁸ J. Ryzka³⁴ J.J. Saborido Silva⁴⁵ N. Sagidova³⁷ N. Sahoo⁵⁵ B. Saitta^{26,f}
 C. Sanchez Gras³¹ C. Sanchez Mayordomo⁴⁶ R. Santacesaria³⁰ C. Santamarina Rios⁴⁵ M. Santimaria²²
 E. Santovetti^{29,j} G. Sarpis⁶¹ A. Sarti³⁰ C. Satriano^{30,s} A. Satta²⁹ M. Saur⁵ D. Savrina^{38,39}
 L.G. Scantlebury Smead⁶² S. Schael¹³ M. Schellenberg¹⁴ M. Schiller⁵⁸ H. Schindler⁴⁷ M. Schmelling¹⁵
 T. Schmelzer¹⁴ B. Schmidt⁴⁷ O. Schneider⁴⁸ A. Schopper⁴⁷ H.F. Schreiner⁶⁴ M. Schubiger³¹ S. Schulte⁴⁸
 M.H. Schune¹¹ R. Schwemmer⁴⁷ B. Sciascia²² A. Sciubba^{30,k} S. Sellam⁶⁸ A. Semennikov³⁸ A. Sergi^{52,47}
 N. Serra⁴⁹ J. Serrano¹⁰ L. Sestini²⁷ A. Seuthe¹⁴ P. Seyfert⁴⁷ D.M. Shangase⁸⁰ M. Shapkin⁴³ L. Shchutka⁴⁸
 T. Shears⁵⁹ L. Shekhtman^{42,x} V. Shevchenko^{76,77} E. Shmanin⁷⁷ J.D. Shupperd⁶⁷ B.G. Siddi²⁰
 R. Silva Coutinho⁴⁹ L. Silva de Oliveira² G. Simi^{27,o} S. Simone^{18,d} I. Skiba²⁰ N. Skidmore¹⁶ T. Skwarnicka⁶⁷
 M.W. Slater⁵² J.G. Smeaton⁵⁴ A. Smetkina³⁸ E. Smith¹³ I.T. Smith⁵⁷ M. Smith⁶⁰ A. Snoch³¹ M. Soares¹⁹
 L. Soares Lavra⁹ M.D. Sokoloff⁶⁴ F.J.P. Soler⁵⁸ B. Souza De Paula² B. Spaan¹⁴ E. Spadaro Norella^{25,q}
 P. Spradlin⁵⁸ F. Stagni⁴⁷ M. Stahl⁶⁴ S. Stahl⁴⁷ P. Stefko⁴⁸ O. Steinkamp⁴⁹ S. Stemmler¹⁶ O. Stenyakin⁴³
 M. Stepanova³⁷ H. Stevens¹⁴ S. Stone⁶⁷ S. Stracka²⁸ M.E. Stramaglia⁴⁸ M. Straticiu³⁶ S. Strovk⁷⁹ J. Sun³
 L. Sun⁷² Y. Sun⁶⁵ P. Svihra⁶¹ K. Swientek³⁴ A. Szabelski³⁵ T. Szumlak³⁴ M. Szymanski⁴⁷ S. Taneja⁶¹
 Z. Tang³ T. Tekampe¹⁴ F. Teubert⁴⁷ E. Thomas⁴⁷ K.A. Thomson⁵⁹ M.J. Tilley⁶⁰ V. Tisserand⁹ S. T'Jampens⁸
 M. Tobin⁶ S. Tolk⁴⁷ L. Tomassetti^{20,g} D. Tonelli²⁸ D. Torres Machado¹ D.Y. Tou¹² E. Tournefier⁸
 M. Traill⁵⁸ M.T. Tran⁴⁸ E. Trifonova⁷⁷ C. Trippi⁴⁸ A. Trisovic⁵⁴ A. Tsaregorodtsev¹⁰ G. Tuci^{28,47,p} A. Tully⁴⁸
 N. Tuning³¹ A. Ukleja³⁵ A. Usachov³¹ A. Ustyuzhanin^{41,78} U. Uwer¹⁶ A. Vagner⁷⁹ V. Vagnoni¹⁹
 A. Valassi⁴⁷ G. Valenti¹⁹ M. van Beuzekom³¹ H. Van Hecke⁶⁶ E. van Herwijnen⁴⁷ C.B. Van Hulse¹⁷
 M. van Veghel⁷⁵ R. Vazquez Gomez^{44,22} P. Vazquez Regueiro⁴⁵ C. Vázquez Sierra³¹ S. Vecchi²⁰ J.J. Velthuis⁵³
 M. Veltri^{21,r} A. Venkateswaran⁶⁷ M. Vernet⁹ M. Veronesi³¹ M. Vesterinen⁵⁵ J.V. Viana Barbosa⁴⁷ D. Vieira⁶⁴
 M. Vieites Diaz⁴⁸ H. Viemann⁷⁴ X. Vilasis-Cardona^{44,m} A. Vitkovskiy³¹ V. Volkov³⁹ A. Vollhardt⁴⁹
 D. Vom Bruch¹² A. Vorobyev³⁷ V. Vorobyev^{42,x} N. Voropaev³⁷ R. Waldi⁷⁴ J. Walsh²⁸ J. Wang³ J. Wang⁷²
 J. Wang⁶ M. Wang³ Y. Wang⁷ Z. Wang⁴⁹ D.R. Ward⁵⁴ H.M. Wark⁵⁹ N.K. Watson⁵² D. Websdale⁶⁰
 A. Weiden⁴⁹ C. Weisser⁶³ B.D.C. Westhenry⁵³ D.J. White⁶¹ M. Whitehead¹³ D. Wiedner¹⁴ G. Wilkinson⁶²
 M. Wilkinson⁶⁷ I. Williams⁵⁴ M. Williams⁶³ M.R.J. Williams⁶¹ T. Williams⁵² F.F. Wilson⁵⁶ W. Wislicki³⁵
 M. Witek³³ L. Witola¹⁶ G. Wormser¹¹ S.A. Wotton⁵⁴ H. Wu⁶⁷ K. Wyllie⁴⁷ Z. Xiang⁵ D. Xiao⁷ Y. Xie⁷
 H. Xing⁷¹ A. Xu⁴ L. Xu³ M. Xu⁷ Q. Xu⁵ Z. Xu⁴ Z. Yang³ Z. Yang⁶⁵ Y. Yao⁶⁷ L.E. Yeomans⁵⁹

H. Yin⁷ J. Yu^{7,aa} X. Yuan⁶⁷ O. Yushchenko⁴³ K.A. Zarebski⁵² M. Zavertyaev^{15,c} M. Zdybal³³ M. Zeng³
 D. Zhang⁷ L. Zhang³ S. Zhang⁴ W.C. Zhang^{3,z} Y. Zhang⁴⁷ A. Zhelezov¹⁶ Y. Zheng⁵ X. Zhou⁵ Y. Zhou⁵
 X. Zhu³ V. Zhukov^{13,39} J.B. Zonneveld⁵⁷ S. Zucchelli^{19,e}

¹Centro Brasileiro de Pesquisas Físicas (CBPF), Rio de Janeiro, Brazil

²Universidade Federal do Rio de Janeiro (UFRJ), Rio de Janeiro, Brazil

³Center for High Energy Physics, Tsinghua University, Beijing, China

⁴School of Physics State Key Laboratory of Nuclear Physics and Technology, Peking University, Beijing, China

⁵University of Chinese Academy of Sciences, Beijing, China

⁶Institute Of High Energy Physics (IHEP), Beijing, China

⁷Institute of Particle Physics, Central China Normal University, Wuhan, Hubei, China

⁸Univ. Grenoble Alpes, Univ. Savoie Mont Blanc, CNRS, IN2P3-LAPP, Annecy, France

⁹Université Clermont Auvergne, CNRS/IN2P3, LPC, Clermont-Ferrand, France

¹⁰Aix Marseille Univ, CNRS/IN2P3, CPPM, Marseille, France

¹¹LAL, Univ. Paris-Sud, CNRS/IN2P3, Université Paris-Saclay, Orsay, France

¹²LPNHE, Sorbonne Université, Paris Diderot Sorbonne Paris Cité, CNRS/IN2P3, Paris, France

¹³I. Physikalisches Institut, RWTH Aachen University, Aachen, Germany

¹⁴Fakultät Physik, Technische Universität Dortmund, Dortmund, Germany

¹⁵Max-Planck-Institut für Kernphysik (MPIK), Heidelberg, Germany

¹⁶Physikalisches Institut, Ruprecht-Karls-Universität Heidelberg, Heidelberg, Germany

¹⁷School of Physics, University College Dublin, Dublin, Ireland

¹⁸INFN Sezione di Bari, Bari, Italy

¹⁹INFN Sezione di Bologna, Bologna, Italy

²⁰INFN Sezione di Ferrara, Ferrara, Italy

²¹INFN Sezione di Firenze, Firenze, Italy

²²INFN Laboratori Nazionali di Frascati, Frascati, Italy

²³INFN Sezione di Genova, Genova, Italy

²⁴INFN Sezione di Milano-Bicocca, Milano, Italy

²⁵INFN Sezione di Milano, Milano, Italy

²⁶INFN Sezione di Cagliari, Monserrato, Italy

²⁷INFN Sezione di Padova, Padova, Italy

²⁸INFN Sezione di Pisa, Pisa, Italy

²⁹INFN Sezione di Roma Tor Vergata, Roma, Italy

³⁰INFN Sezione di Roma La Sapienza, Roma, Italy

³¹Nikhef National Institute for Subatomic Physics, Amsterdam, Netherlands

³²Nikhef National Institute for Subatomic Physics and VU University Amsterdam, Amsterdam, Netherlands

³³Henryk Niewodniczanski Institute of Nuclear Physics Polish Academy of Sciences, Kraków, Poland

³⁴AGH - University of Science and Technology, Faculty of Physics and Applied Computer Science, Kraków, Poland

³⁵National Center for Nuclear Research (NCBJ), Warsaw, Poland

³⁶Horia Hulubei National Institute of Physics and Nuclear Engineering, Bucharest-Magurele, Romania

³⁷Petersburg Nuclear Physics Institute NRC Kurchatov Institute (PNPI NRC KI), Gatchina, Russia

³⁸Institute of Theoretical and Experimental Physics NRC Kurchatov Institute (ITEP NRC KI), Moscow, Russia, Moscow, Russia

³⁹Institute of Nuclear Physics, Moscow State University (SINP MSU), Moscow, Russia

⁴⁰Institute for Nuclear Research of the Russian Academy of Sciences (INR RAS), Moscow, Russia

⁴¹Yandex School of Data Analysis, Moscow, Russia

⁴²Budker Institute of Nuclear Physics (SB RAS), Novosibirsk, Russia

⁴³Institute for High Energy Physics NRC Kurchatov Institute (IHEP NRC KI), Protvino, Russia, Protvino, Russia

⁴⁴ICCUB, Universitat de Barcelona, Barcelona, Spain

⁴⁵Instituto Galego de Física de Altas Enerxías (IGFAE), Universidade de Santiago de Compostela, Santiago de Compostela, Spain

⁴⁶Instituto de Física Corpuscular, Centro Mixto Universidad de Valencia - CSIC, Valencia, Spain

⁴⁷European Organization for Nuclear Research (CERN), Geneva, Switzerland

⁴⁸Institute of Physics, Ecole Polytechnique Fédérale de Lausanne (EPFL), Lausanne, Switzerland

⁴⁹Physik-Institut, Universität Zürich, Zürich, Switzerland

⁵⁰NSC Kharkiv Institute of Physics and Technology (NSC KIPT), Kharkiv, Ukraine

⁵¹Institute for Nuclear Research of the National Academy of Sciences (KINR), Kyiv, Ukraine

⁵²University of Birmingham, Birmingham, United Kingdom

⁵³H.H. Wills Physics Laboratory, University of Bristol, Bristol, United Kingdom

⁵⁴Cavendish Laboratory, University of Cambridge, Cambridge, United Kingdom

⁵⁵Department of Physics, University of Warwick, Coventry, United Kingdom

⁵⁶STFC Rutherford Appleton Laboratory, Didcot, United Kingdom

⁵⁷School of Physics and Astronomy, University of Edinburgh, Edinburgh, United Kingdom

⁵⁸School of Physics and Astronomy, University of Glasgow, Glasgow, United Kingdom

⁵⁹Oliver Lodge Laboratory, University of Liverpool, Liverpool, United Kingdom

⁶⁰Imperial College London, London, United Kingdom

⁶¹Department of Physics and Astronomy, University of Manchester, Manchester, United Kingdom

⁶²Department of Physics, University of Oxford, Oxford, United Kingdom

⁶³Massachusetts Institute of Technology, Cambridge, MA, United States

- ⁶⁴University of Cincinnati, Cincinnati, OH, United States
⁶⁵University of Maryland, College Park, MD, United States
⁶⁶Los Alamos National Laboratory (LANL), Los Alamos, United States
⁶⁷Syracuse University, Syracuse, NY, United States
⁶⁸Laboratory of Mathematical and Subatomic Physics, Constantine, Algeria, associated to ²
⁶⁹School of Physics and Astronomy, Monash University, Melbourne, Australia, associated to ⁵⁵
⁷⁰Pontificia Universidade Católica do Rio de Janeiro (PUC-Rio), Rio de Janeiro, Brazil, associated to ²
⁷¹South China Normal University, Guangzhou, China, associated to ³
⁷²School of Physics and Technology, Wuhan University, Wuhan, China, associated to ³
⁷³Departamento de Física, Universidad Nacional de Colombia, Bogota, Colombia, associated to ¹²
⁷⁴Institut für Physik, Universität Rostock, Rostock, Germany, associated to ¹⁶
⁷⁵Van Swinderen Institute, University of Groningen, Groningen, Netherlands, associated to ³¹
⁷⁶National Research Centre Kurchatov Institute, Moscow, Russia, associated to ³⁸
⁷⁷National University of Science and Technology "MISIS", Moscow, Russia, associated to ³⁸
⁷⁸National Research University Higher School of Economics, Moscow, Russia, associated to ⁴¹
⁷⁹National Research Tomsk Polytechnic University, Tomsk, Russia, associated to ³⁸
⁸⁰University of Michigan, Ann Arbor, United States, associated to ⁶⁷
^aUniversidade Federal do Triângulo Mineiro (UFTM), Uberaba-MG, Brazil
^bLaboratoire Leprince-Ringuet, Palaiseau, France
^cP.N. Lebedev Physical Institute, Russian Academy of Science (LPI RAS), Moscow, Russia
^dUniversità di Bari, Bari, Italy
^eUniversità di Bologna, Bologna, Italy
^fUniversità di Cagliari, Cagliari, Italy
^gUniversità di Ferrara, Ferrara, Italy
^hUniversità di Genova, Genova, Italy
ⁱUniversità di Milano Bicocca, Milano, Italy
^jUniversità di Roma Tor Vergata, Roma, Italy
^kUniversità di Roma La Sapienza, Roma, Italy
^lAGH - University of Science and Technology, Faculty of Computer Science, Electronics and Telecommunications, Kraków, Poland
^mDS4DS, La Salle, Universitat Ramon Llull, Barcelona, Spain
ⁿHanoi University of Science, Hanoi, Vietnam
^oUniversità di Padova, Padova, Italy
^pUniversità di Pisa, Pisa, Italy
^qUniversità degli Studi di Milano, Milano, Italy
^rUniversità di Urbino, Urbino, Italy
^sUniversità della Basilicata, Potenza, Italy
^tScuola Normale Superiore, Pisa, Italy
^uUniversità di Modena e Reggio Emilia, Modena, Italy
^vUniversità di Siena, Siena, Italy
^wMSU - Iligan Institute of Technology (MSU-IIT), Iligan, Philippines
^xNovosibirsk State University, Novosibirsk, Russia
^yINFN Sezione di Trieste, Trieste, Italy
^zSchool of Physics and Information Technology, Shaanxi Normal University (SNNU), Xi'an, China
^{aa}Physics and Micro Electronic College, Hunan University, Changsha City, China
^{ab}Universidad Nacional Autónoma de Honduras, Tegucigalpa, Honduras

Abstract: The production of Ξ_{cc}^{++} baryons in proton-proton collisions at a centre-of-mass energy of $\sqrt{s} = 13$ TeV is measured in the transverse-momentum range $4 < p_T < 15$ GeV/ c and the rapidity range $2.0 < y < 4.5$. The data used in this measurement correspond to an integrated luminosity of 1.7 fb^{-1} , recorded by the LHCb experiment during 2016. The ratio of the Ξ_{cc}^{++} production cross-section times the branching fraction of the $\Xi_{cc}^{++} \rightarrow \Lambda_c^+ K^- \pi^+ \pi^+$ decay relative to the prompt Λ_c^+ production cross-section is found to be $(2.22 \pm 0.27 \pm 0.29) \times 10^{-4}$, assuming the central value of the measured Ξ_{cc}^{++} lifetime, where the first uncertainty is statistical and the second systematic.

Keywords: doubly charmed baryons, hadron production, QCD

DOI: 10.1088/1674-1137/44/2/022001

1 Introduction

The quark model [1,2] predicts the existence of multiplets of baryon and meson states. Baryons containing

two charm quarks and a light quark provide a unique system for testing the low-energy limit of quantum chromodynamics (QCD). The production of doubly charmed baryons at hadron colliders can be treated as two independent processes: production of a cc diquark followed by the

hadronisation of the diquark into a baryon [3-9]. The production cross-section of doubly charmed baryons in proton-proton collisions at a centre-of-mass energy $\sqrt{s} = 13$ TeV is predicted to be in the range 60–1800 nb [3-9], which is between 10^{-4} and 10^{-3} times that of the total charm production [4].

A doubly charmed baryon was first reported by the SELEX collaboration [10,11]. They found that 20% of their Λ_c^+ yield originated from Ξ_{cc}^+ decays, which is several orders of magnitude higher than theoretical prediction [4]. However, this signal has not been confirmed by searches performed at the FOCUS [12], BaBar [13], Belle [14], and LHCb [15,16] experiments. Recently, the LHCb collaboration observed a peak in the $\Lambda_c^+ K^- \pi^+ \pi^+$ mass spectrum at a mass of 3621.40 ± 0.78 MeV/ c^2 [17], consistent with expectations for the Ξ_{cc}^{++} baryon. The Ξ_{cc}^{++} lifetime was measured to be $0.256_{-0.022}^{+0.024}$ (stat) ± 0.014 (syst) ps [18], indicating that it decays through the weak interaction. A new decay mode, $\Xi_{cc}^{++} \rightarrow \Xi_c^+ \pi^+$, was observed by the LHCb collaboration [19], and the measured Ξ_{cc}^{++} mass was found to be consistent with that measured using $\Xi_{cc}^{++} \rightarrow \Lambda_c^+ K^- \pi^+ \pi^+$ decays. The $\Xi_{cc}^{++} \rightarrow D^+ p K^- \pi^+$ decay has been searched for, but no signal was found [20].

This paper presents a measurement of Ξ_{cc}^{++} production in pp collisions at a centre-of-mass energy of $\sqrt{s} = 13$ TeV, following the same analysis strategy as that used in Refs. [15,17,18]. The Ξ_{cc}^{++} production cross-section, $\sigma(\Xi_{cc}^{++})$, times the branching fraction of the $\Xi_{cc}^{++} \rightarrow \Lambda_c^+ K^- \pi^+ \pi^+$ decay, is measured relative to the prompt Λ_c^+ production cross-section, $\sigma(\Lambda_c^+)$, in the transverse momentum range $4 < p_T < 15$ GeV/ c and the rapidity range $2.0 < y < 4.5$. The data used correspond to an integrated luminosity of 1.7 fb^{-1} collected by the LHCb experiment in 2016. The Λ_c^+ baryon is reconstructed via the $\Lambda_c^+ \rightarrow p K^- \pi^+$ decay. The inclusion of the charge-conjugate decay processes is implied throughout this paper. The production rate ratio is defined as,

$$R \equiv \frac{\sigma(\Xi_{cc}^{++}) \times \mathcal{B}(\Xi_{cc}^{++} \rightarrow \Lambda_c^+ K^- \pi^+ \pi^+)}{\sigma(\Lambda_c^+)} = \frac{N_{\text{sig}} \varepsilon_{\text{norm}}}{N_{\text{norm}} \varepsilon_{\text{sig}}}, \quad (1)$$

where “sig” and “norm” refer to the signal (Ξ_{cc}^{++}) and normalisation (Λ_c^+) modes, N is the signal yield and ε is the total efficiency to reconstruct and select these decays.

2 Detector and simulation

The LHCb detector [21,22] is a single-arm forward spectrometer covering the pseudorapidity range $2 < \eta < 5$, designed for the study of particles containing b or c quarks. The detector includes a high-precision tracking system consisting of a silicon-strip vertex detector surrounding the pp interaction region [23], a large-area silicon-strip detector located upstream of a dipole magnet

with a bending power of about 4 Tm, and three stations of silicon-strip detectors and straw drift tubes [24] placed downstream of the magnet. The tracking system provides a measurement of the momentum, p , of charged particles with a relative uncertainty that varies from 0.5% at low momentum to 1.0% at 200 GeV/ c . The minimum distance of a track to a primary vertex, the impact parameter, is measured with a resolution of $(15 + 29/p_T)$ μm , where p_T is expressed in GeV/ c . Different types of charged hadrons are distinguished using information from two ring-imaging Cherenkov detectors [25]. Photons, electrons and hadrons are identified by a calorimeter system consisting of scintillating-pad (SPD) and preshower detectors, an electromagnetic and a hadronic calorimeter. Muons are identified by a system composed of alternating layers of iron and multiwire proportional chambers [26]. The online event selection is performed by a trigger [27], which consists of a hardware stage, based on information from the calorimeters and muon systems [28,29], followed by a software stage, which applies a full event reconstruction incorporating near-real-time alignment and calibration of the detector [30]. The output of the reconstruction performed in the software trigger [31] is used as input to the present analysis.

Simulated samples are required to develop the candidate selection and to estimate the efficiency of the detector acceptance and the imposed selection requirements. Simulated pp collisions are generated using PYTHIA [32] with a specific LHCb configuration [33]. A dedicated package, GENXICC2.0 [34], is used to simulate the Ξ_{cc}^{++} baryon production. Decays of unstable particles are described by EVTGEN [35], in which final-state radiation is generated using PHOTOS [36]. The interaction of the generated particles with the detector, and its response, are simulated using the GEANT4 toolkit [37] as described in Ref. [38].

3 Event selection

The $\Lambda_c^+ \rightarrow p K^- \pi^+$ candidate is reconstructed through three charged particles identified as p , K^- and π^+ hadrons, which form a common vertex and do not originate from any primary vertex (PV) in the event. The decay vertex of the Λ_c^+ candidate is required to be displaced from any PV by requiring its proper decay time to be greater than 0.15 ps, corresponding to about 1.5 times the Λ_c^+ decay time resolution [39]. Each Λ_c^+ candidate with mass in the range 2270–2306 MeV/ c^2 is then combined with three additional particles to form a Ξ_{cc}^{++} candidate. The three particles must form a common vertex with the Λ_c^+ candidate and have hadron-identification information consistent with them being two π^+ mesons and one K^- meson. The Λ_c^+ decay vertex is required to be downstream of the Ξ_{cc}^{++} ver-

tex. Additionally, the Ξ_{cc}^{++} candidates must have $p_T > 4 \text{ GeV}/c$ and originate from a PV.

The combinatorial background is suppressed using two multivariate classifiers based on a boosted decision tree algorithm [40]. One classifier is optimised to select Λ_c^+ candidates irrespective of their origin, and the other is optimised to select Ξ_{cc}^{++} candidates. While both classifiers are applied to the signal channel, only the first is applied to the normalisation decay channel. The first classifier is trained with Λ_c^+ signal in the simulated Ξ_{cc}^{++} sample and background candidates in the Λ_c^+ mass sideband. The second classifier is trained using data candidates in the Λ_c^+ and Ξ_{cc}^{++} signal mass region, where wrong-sign (WS) $\Lambda_c^+ K^- \pi^+ \pi^-$ combinations are used as proxy for the background. The first multivariate classifier is trained with the following variables: the χ^2 of the Λ_c^+ vertex fit; the largest distance of closest approach among the decay products; the scalar sum of the p_T and the smallest p_T of the three decay products of the Λ_c^+ candidate; the smallest and largest χ_{IP}^2 of the decay products of the Λ_c^+ candidate with respect to its PV. Here, χ_{IP}^2 is defined as the difference in χ^2 of the PV fit with and without the particle in question. The PV of any single particle is defined to be that with respect to which the particle has the smallest χ_{IP}^2 . The second multivariate classifier is trained with the following variables: the χ_{IP}^2 of the Ξ_{cc}^{++} candidate to its PV; the angle between the Ξ_{cc}^{++} momentum and the direction from the PV to the Ξ_{cc}^{++} decay vertex; the logarithm of the χ^2 of the Ξ_{cc}^{++} flight distance between the Ξ_{cc}^{++} decay vertex and the PV; the vertex fit χ^2 of the Ξ_{cc}^{++} candidate; the χ^2 of a kinematic refit [41] that requires the Ξ_{cc}^{++} candidate to originate from a PV; the scalar sum of the p_T and the smallest p_T of the six final state tracks of the Ξ_{cc}^{++} candidate. Here the flight distance χ^2 is defined as the change in χ^2 of the Ξ_{cc}^{++} decay vertex if it is constrained to coincide with the PV. Candidates retained for analysis must have two classifier responses exceeding thresholds chosen by performing a two-dimensional maximisation of the figure of merit $\varepsilon/(5/2 + \sqrt{B})$ [42]. Here ε and B are the estimated signal efficiency determined from signal simulation and background yield under the signal peak, respectively. The background is estimated from the WS sample. The same threshold of the first classifier, optimised for the signal mode, is applied to the normalisation mode.

Finally, the Ξ_{cc}^{++} and Λ_c^+ candidates are required to have their transverse momentum and rapidity in the fiducial ranges of 4-15 GeV/c and 2.0-4.5, respectively. After the multivariate selection is applied, events may still contain more than one Ξ_{cc}^{++} candidate in the signal region. Candidates made of duplicate tracks are removed by requiring all pairs of tracks with the same charge to have an opening angle larger than 0.5 mrad. Duplicate candidates, which are due to the interchange between identical

particles from the Λ_c^+ decay or directly from the Ξ_{cc}^{++} decay (e.g., the K^- particle from the Ξ_{cc}^{++} decay and the K^- particle from the Λ_c^+ decay), can cause peaking structures in the Ξ_{cc}^{++} invariant mass distribution. In this case, one of the candidates is chosen at random to be retained and the others are discarded. The systematic uncertainty associated with this procedure is negligible.

4 Signal yields

After the full selection is applied, the data sets are further filtered into two disjoint subsamples using information from the hardware trigger. The first contains candidates that are triggered by at least one of the Λ_c^+ decay products with high transverse energy deposited in the calorimeters, referred to as Triggered On Signal (TOS). The second consists of the events that are exclusively triggered by particles unrelated to the signal decay products; these events can, for example, be triggered by the decay products of the charmed hadrons produced together with the signal baryon, referred to as exclusively Triggered Independently of Signal (exTIS).

To determine the Ξ_{cc}^{++} baryon signal yields, an unbinned extended maximum-likelihood fit is performed simultaneously to the $\Lambda_c^+ K^- \pi^+ \pi^+$ invariant-mass spectra in the interval 3470-3770 MeV/c^2 of the two trigger categories. The mass distribution of the signal is described by the sum of a Gaussian function and a modified Gaussian function with power-law tails on both sides of the function [43] with a common peak position. The tail parameters and the relative fraction of the two Gaussian functions for the signal model are determined from simulation, while the common peak position and the mass resolution are allowed to vary in the fit. The background is described by a second-order Chebyshev polynomial. Fig. 1 shows the $\Lambda_c^+ K^- \pi^+ \pi^+$ invariant-mass distribution in data together with the fit results for the two trigger categories. The fit returns a mass of $3621.34 \pm 0.74 \text{ MeV}/c^2$, and a mass resolution of $7.1 \pm 1.3 \text{ MeV}/c^2$, where the uncertainties are statistical only.

The determination of the prompt Λ_c^+ baryon yields, which are contaminated by Λ_c^+ candidates produced in b -hadron decays, is done in two steps [44]. First, a binned extended maximum-likelihood fit to the $m(pK^- \pi^+)$ invariant-mass distribution in the interval 2220-2360 MeV/c^2 is performed to determine the total number of Λ_c^+ candidates. Then a binned extended maximum-likelihood fit to the background-subtracted $\log_{10}(\chi_{IP}^2(\Lambda_c^+))$ distribution is performed to separate the prompt Λ_c^+ component from that originated in b -hadron decays. The mass distribution of Λ_c^+ candidates is described by a sum of a Gaussian function and a modified Gaussian function with power-law tails on both sides with a common peak position. The

background mass distribution is described by a first-order Chebyshev polynomial. The $\log_{10}(\chi_{\text{IP}}^2(\Lambda_c^+))$ distribution, after subtracting the combinatorial background using the *sPlot* technique [45], is described by two Bukin functions [46]. All the parameters except the peak position and resolution of the functions are derived from a fit

to simulated signal. Figs. 2 and 3 show the $pK^-\pi^+$ invariant-mass distribution and $\log_{10}(\chi_{\text{IP}}^2(\Lambda_c^+))$ distributions in data together with the fit results for the two trigger categories. The signal yields for both the signal and the normalisation modes are presented in Table 1.

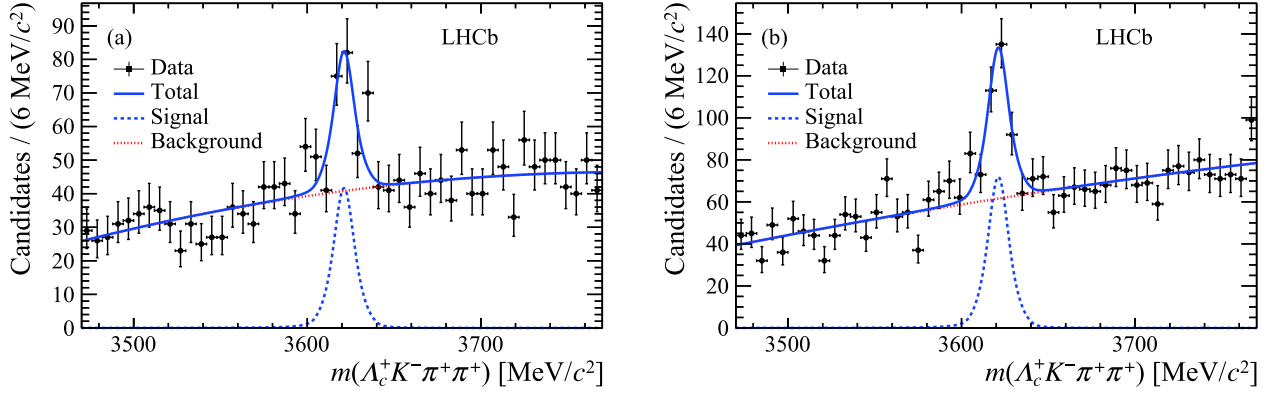


Fig. 1. (color online) Invariant-mass distributions of Ξ_{cc}^+ candidates (a) triggered by TOS and (b) triggered by exTIS, with fit results shown.

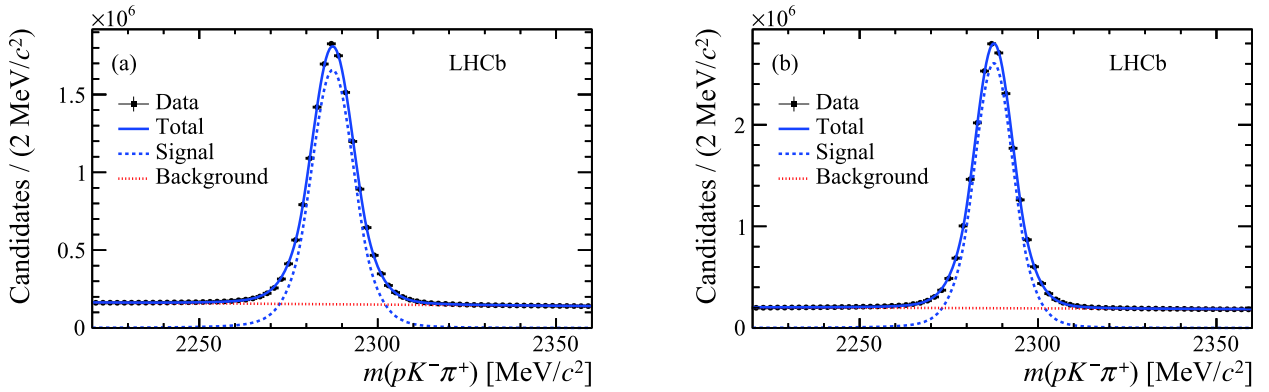


Fig. 2. (color online) Invariant-mass distributions of Λ_c^+ candidates (a) triggered by TOS and (b) triggered by exTIS, with fit results shown.

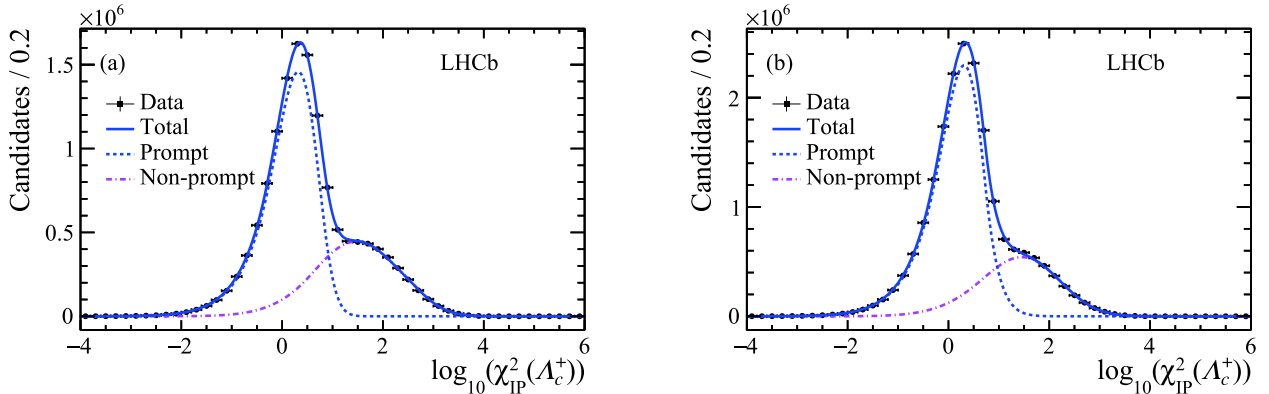


Fig. 3. (color online) Distributions of $\log_{10}(\chi_{\text{IP}}^2(\Lambda_c^+))$ for background-subtracted candidates (a) triggered by TOS and (b) triggered by exTIS, with fit results shown.

Table 1. Yields of the signal and normalisation modes.

Category	N_{sig}	$N_{\text{norm}} [10^3]$
TOS	116 ± 23	8764 ± 6
exTIS	210 ± 29	13889 ± 8

5 Efficiencies

For each trigger category and for both the signal and the normalisation channels, the total efficiencies are computed as products of the detector geometrical acceptance and of the efficiencies related to particle reconstruction, event selection, particle identification and trigger. All the efficiencies are calculated using simulation that is corrected using data. For both the signal and the normalisation modes, the kinematic distributions in simulation samples, including the transverse momentum and rapidity of the Ξ_{cc}^{++} and Λ_c^+ baryons and the event multiplicity, are weighted to match those in the corresponding data. The efficiencies are calculated under three lifetime ($\tau_{\Xi_{cc}^{++}}$) hypotheses: the central value of the measured lifetime, and the lifetime increased or decreased by its measured uncertainty [18]. The dependence of the efficiency on the Ξ_{cc}^{++} baryon lifetime is almost linear, with the efficiency ratio varying by 25% from the lower lifetime to the higher one. The resonant structures of the $\Lambda_c^+ \rightarrow pK^-\pi^+$ decay are also weighted based on the background-subtracted data, as the simulation samples do not model well the structure seen in the data. The tracking efficiency is corrected with control data samples, as described in Ref. [47]. The particle-identification efficiency is corrected in bins of particle momentum, pseudorapidity and event multiplicity, using the results of a tag-and-probe method applied to calibration samples [48]. The efficiency ratios of the normalisation mode to the signal mode are presented in Table 2.

Table 2. Ratios of the normalisation and signal efficiencies.

Category	$\epsilon_{\text{norm}}/\epsilon_{\text{sig}}$		
	$\tau_{\Xi_{cc}^{++}} = 0.230$ ps	$\tau_{\Xi_{cc}^{++}} = 0.256$ ps	$\tau_{\Xi_{cc}^{++}} = 0.284$ ps
TOS	22.00 ± 1.09	19.50 ± 1.71	17.50 ± 1.50
exTIS	16.64 ± 1.30	14.56 ± 1.06	12.95 ± 0.80

6 Systematic uncertainties

The sources of systematic uncertainties affecting the measurement of the production ratio include the choice of the fit model and the evaluation of the total efficiency. The uncertainties are summarised in Table 3.

For both the signal and normalisation modes, the uncertainties due to the choice of the particular fit model are estimated by using alternative functions where the signal

Table 3. Relative systematic uncertainties on the production ratio measurement for the two trigger categories.

Source	TOS [%]	exTIS [%]
Simulation sample size	8.8	7.3
Fit model	5.4	5.3
Hardware trigger	9.0	6.3
Tracking	3.4	3.4
Particle identification	5.5	5.4
Kinematic correction	7.3	6.0
Sum in quadrature	16.8	14.1

is described by a sum of two Gaussian functions with a common peak position and the background is described by a second-order polynomial function. The difference in the ratio of signal yields between the two fits is assigned as systematic uncertainty. Additional effects coming from the $\log_{10}(\chi_{\text{IP}}^2(\Lambda_c^+))$ fit are tested with alternative functions where the parameters used to describe the nonprompt signal are determined from a Λ_b^0 baryon data sample. The effect from the background subtraction is studied using the shape determined with the candidates in the Λ_c^+ baryon mass sidebands.

The limited size of the simulation samples leads to systematic uncertainties on the efficiencies. The systematic uncertainty due to the trigger selection efficiency is estimated with a tag-and-probe method exploiting a sample of events that are also triggered by particles unrelated to the signal candidate [27]. Due to the small sample size of the signal channel in data, two different control samples are used. The first sample comprises $\Lambda_b^0 \rightarrow \Lambda_c^+ \pi^- \pi^+ \pi^-$ decays, which are topologically similar to the $\Xi_{cc}^{++} \rightarrow \Lambda_c^+ K^- \pi^+ \pi^+$ decay. The second sample comprises $B_c^+ \rightarrow J/\psi \pi^+$ decays. This decay does not have the same topology but shares another feature with the signal: there should be at least two other heavy-flavour particles (b - or c -hadrons) produced in the same event that can be responsible for the trigger decision. The hardware trigger efficiencies of the Λ_b^0 , B_c^+ decay channels and prompt Λ_c^+ channel, are measured using the tag-and-probe method. Similar selections to those applied to the signal channel are applied to both the data and simulation for the control samples. The efficiency ratio of the Λ_b^0 , B_c^+ decays to the Λ_c^+ decays is estimated and the difference of the ratio in data and in simulation is assigned as a systematic uncertainty. The transverse-energy threshold in the calorimeter hardware trigger varied during data taking, and this variation is not fully described by the simulation. The threshold used in the simulated samples is higher than that applied to some data. To investigate the influence of this difference, the same hardware trigger requirement used in the simulation is applied to the data. The meas-

urement is repeated and the change in the measured production ratio is taken as a systematic uncertainty.

The systematic uncertainty related to the tracking efficiency includes three effects. First, the tracking efficiency depends on the detector occupancy, which is not well described by simulation. The distribution of the number of SPD hits in simulated samples is weighted to match that in data and an uncertainty of 0.8% per track is assigned to account for remaining difference in multiplicity between data and simulation [47]. Secondly, the uncertainty due to the finite size of the control samples is propagated to the final systematic uncertainty using a large number of pseudoexperiments. Finally, an uncertainty is assigned to the track reconstruction efficiency due to uncertainties on the material budget of the detector and on the modelling of hadronic interaction with the detector material.

The systematic uncertainty related to the particle-identification efficiency includes three effects. The effect from the limited size of calibration samples is evaluated with a large number of pseudoexperiments. Effects of binning in momentum, pseudorapidity and event multiplicity is evaluated by increasing or decreasing the bin sizes by a factor of two. In this estimation, the effects of the correlations between tracks on the particle identification performance are taken into account using simulated samples.

The uncertainties on the weights used for the correction of the kinematic distributions of the simulation samples are propagated as a systematic uncertainty on the production ratio.

7 Results

The production-rate ratio is calculated for the TOS and the exTIS categories of events for three different Ξ_{cc}^{++} lifetime scenarios using Eq. (1). The separate ratios in the TOS and exTIS categories are presented in Table 4 and are found to be consistent. The combination of the trig-

Table 4. Production rate ratio results for three different Ξ_{cc}^{++} lifetime hypotheses. The first uncertainty is statistical and the second is systematic.

Category	$R [10^{-4}]$		
	$\tau_{\Xi_{cc}^{++}} = 0.230$ ps	$\tau_{\Xi_{cc}^{++}} = 0.256$ ps	$\tau_{\Xi_{cc}^{++}} = 0.284$ ps
TOS	$2.90 \pm 0.57 \pm 0.49$	$2.57 \pm 0.51 \pm 0.43$	$2.31 \pm 0.46 \pm 0.39$
exTIS	$2.41 \pm 0.35 \pm 0.34$	$2.11 \pm 0.31 \pm 0.30$	$1.88 \pm 0.27 \pm 0.27$
Combined	$2.53 \pm 0.30 \pm 0.33$	$2.22 \pm 0.27 \pm 0.29$	$1.98 \pm 0.23 \pm 0.26$

ger categories, using the Best Linear Unbiased Estimate method [49] is also reported. In the combination, the systematic uncertainties coming from the simulation sample size and hardware trigger are assumed to be uncorrelated, while the other systematic uncertainties are considered to be 100% correlated.

8 Conclusion

A first measurement of the Ξ_{cc}^{++} production cross-section relative to that of Λ_c^+ baryons is presented. The ratio of Ξ_{cc}^{++} production cross-section times the branching fraction of the $\Xi_{cc}^{++} \rightarrow \Lambda_c^+ K^- \pi^+ \pi^+$ decay relative to the prompt Λ_c^+ production cross-section in the kinematic region $4 < p_T < 15$ GeV/c and $2.0 < y < 4.5$ is measured to be $(2.22 \pm 0.27 \pm 0.29) \times 10^{-4}$, assuming the central value of the Ξ_{cc}^{++} lifetime measured in Ref. [18], where the first uncertainty is statistical and the second systematic. This is the first measurement of the production of the doubly charmed baryons in pp collisions and will deepen our understanding on their production mechanism.

We thank Chao-Hsi Chang, Cai-Dian Lü, Xing-Gang Wu, and Fu-Sheng Yu for the discussions on the production and decays of double-heavy-flavour baryons. We express our gratitude to our colleagues in the CERN accelerator departments for the excellent performance of the LHC. We thank the technical and administrative staff at the LHCb institutes.

References

- M. Gell-Mann, *Phys. Lett.*, **8**: 214 (1964)
- G. Zweig, Tech. Rep. CERN-TH-401, CERN, Geneva, 1964
- A. V. Berezhnoy, V. V. Kiselev, A. K. Likhoded et al, *Phys. Rev. D*, **57**: 4385 (1998), arXiv:[hep-ph/9710339](#)
- V. V. Kiselev and A. K. Likhoded, *Phys. Usp.*, **45**: 455 (2002), arXiv:[hep-ph/0103169](#)
- J. P. Ma and Z. G. Si, *Phys. Lett. B*, **568**: 135 (2003), arXiv:[hep-ph/0305079](#)
- C.-H. Chang, J.-P. Ma, C.-F. Qiao et al, *J. Phys. G*, **34**: 845 (2007), arXiv:[hep-ph/0610205](#)
- C.-H. Chang, C.-F. Qiao, J.-X. Wang et al, *Phys. Rev. D*, **73**: 094022 (2006), arXiv:[hep-ph/0601032](#)
- J.-W. Zhang et al, *Phys. Rev. D*, **83**: 034026 (2011), arXiv:[1101.1130](#)
- C.-H. Chang, C.-F. Qiao, J.-X. Wang et al, *Phys. Rev. D*, **71**: 074012 (2005), arXiv:[hep-ph/0502155](#)
- SELEX Collaboration, M. Mattson et al, *Phys. Rev. Lett.*, **89**: 112001 (2002), arXiv:[hep-ex/0208014](#)
- SELEX Collaboration, A. Ocherashvili et al, *Phys. Lett. B*, **628**: 18 (2005), arXiv:[hep-ex/0406033](#)
- S. P. Ratti et al, *Nucl. Phys. Proc. Suppl.*, **115**: 33 (2003)
- BaBar Collaboration, B. Aubert et al, *Phys. Rev. D*, **74**: 011103 (2006), arXiv:[hep-ex/0605075](#)
- Belle Collaboration, R. Chistov et al, *Phys. Rev. Lett.*, **97**: 162001 (2006), arXiv:[hep-ex/0606051](#)
- LHCb Collaboration, R. Aaij et al, *JHEP*, **12**: 090 (2013), arXiv:[1310.2538](#)
- LHCb Collaboration, R. Aaij et al, *Sci. China-Phys. Mech.*

- Astron., **63**: 221062 (2020), arXiv: 1909.12273
- 17 LHCb Collaboration, R. Aaij et al, *Phys. Rev. Lett.*, **119**: 112001 (2017), arXiv:1707.01621
- 18 LHCb Collaboration, R. Aaij et al, *Phys. Rev. Lett.*, **121**: 052002 (2018), arXiv:1806.02744
- 19 LHCb Collaboration, R. Aaij et al, *Eur. Phys. J. C*, **78**: 443 (2018), arXiv:1712.08609
- 20 LHCb Collaboration, R. Aaij et al, *JHEP*, **10**: 124 (2019), arXiv:1905.02421
- 21 LHCb Collaboration, A. A. Alves Jr. et al, *JINST*, **3**: S08005 (2008)
- 22 LHCb Collaboration, R. Aaij et al, *Int. J. Mod. Phys. A*, **30**: 1530022 (2015), arXiv:1412.6352
- 23 R. Aaij et al, *JINST*, **9**: P09007 (2014), arXiv:1405.7808
- 24 P. d'Argent et al, *JINST*, **12**: P11016 (2017), arXiv:1708.00819
- 25 M. Adinolfi et al, *Eur. Phys. J. C*, **73**: 2431 (2013), arXiv:1211.6759
- 26 A. A. Alves Jr. et al, *JINST*, **8**: P02022 (2013), arXiv:1211.1346
- 27 R. Aaij et al, *JINST*, **8**: P04022 (2013), arXiv:1211.3055
- 28 R. Aaij et al, LHCb-DP-2013-004, in preparation
- 29 F. Archilli et al, *JINST*, **8**: P10020 (2013), arXiv:1306.0249
- 30 R. Aaij et al, *JINST*, **14**: P04013 (2019), arXiv:1812.10790
- 31 R. Aaij et al, *Comput. Phys. Commun.*, **208**: 35 (2016), arXiv:1604.05596
- 32 T. Sjöstrand, S. Mrenna, and P. Skands, *Comput. Phys. Commun.*, **178**: 852 (2008), arXiv: 0710.3820; T. Sjöstrand, S. Mrenna, and P. Skands, *JHEP* **05**: 026 (2006), arXiv: hep-ph/0603175
- 33 I. Belyaev et al, *J. Phys. Conf. Ser.*, **331**: 032047 (2011)
- 34 C.-H. Chang, J.-X. Wang, and X.-G. Wu, *Comput. Phys. Commun.*, **181**: 1144 (2010), arXiv:0910.4462
- 35 D. J. Lange, *Nucl. Instrum. Meth. A*, **462**: 152 (2001)
- 36 P. Golonka and Z. Was, *Eur. Phys. J. C*, **45**: 97 (2006), arXiv:hep-ph/0506026
- 37 Geant4 Collaboration, J. Allison et al, *IEEE Trans. Nucl. Sci.*, **53**: 270 (2006); Geant4 Collaboration, S. Agostinelli et al, *Nucl. Instrum. Meth. A*, **506**: 250 (2003)
- 38 M. Clemencic et al, *J. Phys. Conf. Ser.*, **331**: 032023 (2011)
- 39 Particle Data Group, M. Tanabashi et al, *Phys. Rev. D*, **98**: 030001 (2018)
- 40 H. Voss, A. Hoecker, J. Stelzer et al, *PoS ACAT (2007) 040*; A. Hoecker et al, *TMVA 4- Toolkit for Multivariate Data Analysis with ROOT. Users Guide.*, arXiv: physics/0703039
- 41 W. D. Hulsbergen, *Nucl. Instrum. Meth. A*, **552**: 566 (2005), arXiv:physics/0503191
- 42 G. Punzi, eConf, **C030908**: MODT002 (2003), arXiv:physics/0308063
- 43 T. Skwarnicki, PhD thesis, Institute of Nuclear Physics, Krakow, 1986, DESY-F31-86-02
- 44 LHCb Collaboration, R. Aaij et al, *Nucl. Phys. B*, **871**: 1 (2013), arXiv:1302.2864
- 45 M. Pivk and F. R. Le Diberder, *Nucl. Instrum. Meth. A*, **555**: 356 (2005), arXiv:physics/0402083
- 46 A. D. Bukin, arXiv: 0711.4449
- 47 LHCb Collaboration, R. Aaij et al, *JINST*, **10**: P02007 (2015), arXiv:1408.1251
- 48 R. Aaij et al, *Eur. Phys. J. Tech. Instr.*, **6**: 1 (2018), arXiv:1803.00824
- 49 R. Nisius, *Eur. Phys. J. C*, **74**: 3004 (2014), arXiv: 1402.4016; R. Nisius, *Blue: a software package to combine correlated estimates of physics observables within root using the best linear unbiased estimate method - program manual, version 2.1.0*, <http://blue.hepforge.org>.